The Astronomical Journal, 133:2669–2678, 2007 June

PROPERTIES OF THE ζ AUR–TYPE BINARY SYSTEM 22 VUL = QS VUL

Joel A. Eaton and Felecia G. Shaw
Center of Excellence in Information Systems, Tennessee State University, Nashville, TN 37209, USA; eaton@donne.tsuniv.edu
Received 2006 March 29; accepted 2006 December 21

ABSTRACT

The 22 Vul system is important for studying the winds and chromospheres of cool evolved stars because the G4 I component is rotating rapidly and probably faster than synchronously. We discuss the system's physical properties in the context of a wide range of constraints on them and propose values that may be marginally better than previous ones (see the end of § 3). We use Hα spectroscopy to assess the variability of the cool star's wind, and archival *IUE* observations to measure variation of density in the wind and rotation of the chromosphere. We argue that the terminal velocity of the wind must be at least as great as the edge velocity of Mg II and derive a new value of $v_\infty \gtrsim 208 \pm 5$ km s^{-1}. Directly measured column densities for hydrogen (from Lyα), combined with column densities for metals, imply a $\beta \sim 2.5$ velocity law for the wind with a mass-loss rate of $\sim 1.6 \times 10^{-8}\ M_\odot$ yr^{-1}, about 4 times the surface flux of 31 Cyg. Excitation temperatures and turbulent velocities in the inner $3R_*$ of the wind are similar to those in other ζ Aur binaries. The apparent faster-than-synchronous rotation Griffin and coworkers found in the optical persists in *IUE* spectra out to at least $2.5R$(G4 I). This implies that the wind is locked to the star through magnetic fields or that the material in the wind is viscous enough to maintain approximately solid-body rotation.

Key words: binaries: eclipsing — stars: late-type — stars: winds, outflows

Online material: machine-readable tables

1. INTRODUCTION

The ζ Aurigae binaries (Wright 1970) give us a unique window into the processes of chromospheric emission and mass loss in cool supergiant stars. These systems consist of a cool supergiant paired with a B dwarf, the prototype system ζ Aur consisting of K4 Ib and B5 V components. Absorptions in the spectrum of the B star by the gas in the wind and chromosphere of the K star give us a spatial probe of the K star's wind. The three classical systems, ζ Aur, 32 Cyg, and 31 Cyg, have long periods, large separations, and supergiant K primaries. They are probably good surrogates for single-star evolution in that their appreciable orbital eccentricities mean the K components have never been close to their Roche lobes.

Unlike the classical ζ Aur binaries, the system 22 Vul (G4 I + B9 V, $P = 249$ days) is close enough that it might be tidally locked. Furthermore, the star's circular orbit suggests that the primary has been close to its Roche lobe in the past and that the system could even have suffered limited mass exchange (see Abt [2006] for a discussion of circularization in cool giants). The supergiant component thereby probably rotates much faster than it would as a single star. It is thus a prime candidate for a star with elevated magnetic activity, whatever form that would take in a *supergiant*, so observation of this system is desirable for studying the effect of rapid rotation among the cool giants with massive winds.

Because this system is potentially significant for both stellar evolution and wind theory of cool giants/supergiants, it is important to know the masses, radii, and temperatures of the components and the mass-loss rate and density-velocity-temperature structure of the primary's wind as precisely as possible. These parameters are absolute requirements for placing the star reliably in the H-R diagram and determining how it got to its present state. Yet they are not yet known well enough to do so.

There are a number of very good observational studies of the 22 Vul system, but the quality of their results is limited by complications intrinsic to the system itself. Parsons et al. (1985) used optical photometry and spectra to show that 22 Vul eclipses completely, to determine that its orbit is circular, and to establish its period. Griffin et al. (1993) did a comprehensive analysis of radial velocities, optical high-dispersion spectra, and photometry to define the system's properties as precisely as possible for the data then available. A highlight of their work was measuring the mass ratio crudely, $q = M(\text{G4 I})/M(\text{B9 V}) = 1.6 \pm 0.2$ from shifts of the B component's Balmer lines in optical spectra. We ourselves have previously detected 22 Vul's ellipsoidal light variation and measured the rotational velocity of its primary, $v \sin i = 17 \pm 2$ km s^{-1} (Eaton et al. 1994). This rotational velocity, derived from metallic lines near Hα (see Eaton [1990] for a discussion of the technique), agrees moderately well with some previous values, which were nearer 15 km s^{-1}, and implies a rather large radius ($84.8 \pm 10\ R_\odot$) for synchronous rotation. The most surprising result for this star is the conclusion of Griffin et al. that the chromosphere is rotating *faster* than synchronously. This is somewhat surprising in that the synchronization time is generally much shorter than the orbital circularization time, and in that our general prejudice is that ζ Aur binaries have not suffered Roche lobe overflow. However, this evidence would give us unique insights about how chromospheres and winds are structured and driven, once we figure out how to interpret it. Complicating this analysis is the fact that a rotation measured in the low chromosphere is merely another way of measuring the value of $v \sin i$ for the star, and the values given by Griffin et al. (1993, Table 5, col. [3]), absent a zero-point error, fall at the upper end of the values of $v \sin i$ measured from line broadening.

To understand the G supergiant in 22 Vul better, we have obtained optical observations to refine the parameters of the 22 Vul binary system. These consist of a series of red high-dispersion spectra, to give radial velocities and profiles of Hα, and 8 years' *BV* photometry to define the light variation outside eclipse, so as to use it to restrict values of mass ratio and radius of the primary. We also report an analysis of archival *IUE* observations in the atmospheric eclipses.

2. SPECTRA AND RADIAL VELOCITIES

We collected two sets of high-dispersion spectra over the years. First, we have data from the stellar spectrograph of the

TABLE 1
Optical Spectra for 22 Vul from the AST

Date (HJD−2,400,000)	RV (km s^{-1})	EW1 (Å)	EW2 (Å)	Date (HJD−2,400,000)	RV (km s^{-1})	EW1 (Å)	EW2 (Å)
52868.7734	−28.4	1.824	0.170	53186.8906	−6.8	1.794	0.096
52869.9648	−28.1	1.887	0.186	53187.8867	−6.0	1.912	0.110
52871.8711	−26.2	1.856	0.159	53188.8867	−5.2	1.790	0.075
52895.7070	−8.7	1.807	0.131	53189.7852	−3.7	1.786	0.079
52896.7148	−8.0	1.787	0.140	53190.8750	−3.5	1.904	0.087
52897.7031	−7.0	1.724	0.161	53191.8750	−2.7	1.849	0.097
52898.7148	−5.8	1.750	0.170	53192.8711	−1.7	1.586	0.064
52899.6758	−5.3	1.747	0.168	53193.7695	−0.5	...	...
52900.6719	−4.5	1.799	0.205	53198.8555	3.5	1.807	0.132
52901.7109	−3.0	1.691	0.198	53203.8047	7.2	...	0.094
52903.7109	−1.4	1.816	0.253	53208.6914	9.4	...	0.086
52904.6641	−0.7	1.758	0.270	53208.8008	11.1	...	...
52908.7188	−3.0	1.866	0.292	53212.7734	13.9	1.810	0.142
52909.7148	4.1	1.935	0.307	53216.6875	20.1	1.824	0.169
52910.7031	5.0	1.887	0.294	53228.8203	10.8	1.739	0.191
52911.6992	5.9	...	0.274	53243.8984	14.2	1.763	0.290
52912.6992	6.8	1.904	0.282	53244.9297	13.7	1.728	0.282
52913.7227	7.7	1.870	0.275	53247.8984	14.7	...	0.292
52914.7070	−4.1	...	0.248	53250.8516	14.4	...	...
52916.6914	−2.3	1.896	0.226	53258.8828	14.2	...	...
52917.7070	−1.5	1.905	0.189	53261.6875	9.2	2.133	0.199
52918.7031	−0.5	1.923	0.203	53262.8828	12.4	1.851	0.177
52926.6758	7.4	...	0.183	53263.6797	11.9	2.174	0.198
52952.6289	23.9	...	...	53264.8750	12.1	2.076	0.201
53045.0352	−25.2	1.830	0.136	53265.7031	10.8	2.130	0.190
53046.0352	−25.9	1.889	0.114	53270.6562	9.0	1.987	0.154
53061.9844	−30.1	1.642	0.157	53271.7227	8.8	1.939	0.148
53085.0078	−48.3	...	0.140	53272.6484	8.4	1.975	0.160
53086.9922	−49.7	...	0.105	53274.7656	7.4	1.844	0.149
53095.8867	−53.6	1.713	0.220	53279.6680	5.5	1.825	0.118
53114.9453	−55.9	1.916	0.150	53281.7812	4.9	1.804	0.110
53120.8320	−54.9	1.780	0.143	53282.7070	4.2	1.806	0.107
53131.7852	−50.9	...	...	53288.7266	1.4	1.946	0.167
53132.7852	−50.3	1.585	0.171	53293.7031	−1.4	1.937	0.182
53134.7773	−50.1	...	...	53301.7070	−5.8	1.868	0.096
53135.7734	−49.2	1.677	0.119	53309.7539	−9.6	1.799	0.119
53136.9531	−48.7	1.849	0.183	53315.6289	−36.4	1.777	0.124
53137.7656	−45.8	1.670	0.160	53329.6875	−43.2	1.822	0.112
53138.7695	−47.7	1.701	0.153	53340.6094	−46.4	1.998	0.148
53145.9219	−42.9	1.738	0.105	53351.6055	−48.2	2.012	0.176
53148.9766	−39.8	...	...	53357.5977	−48.0	1.758	0.201
53172.9219	−19.9	1.763	0.117	53416.0000	−20.9	1.963	0.132
53173.8906	−19.0	1.735	0.109	53424.9922	−14.9	1.929	0.144
53174.8945	−18.2	1.758	0.121	53532.9492	−15.6	2.256	0.304
53175.8867	−17.4	1.767	0.116	53551.9766	−28.5	2.337	0.287
53176.8633	−16.1	1.747	0.137	53564.8711	−36.6	1.952	0.114
53177.9180	−15.4	1.747	0.151	53610.8945	−47.3	1.693	0.128
53180.9062	−12.6	1.852	0.130	53632.7812	−40.6	1.874	0.165
53183.8906	−9.7	1.710	0.095	53674.7148	−14.5	1.785	0.134
53184.8945	−8.9	1.816	0.069				

Note.—Table 1 is also available in machine-readable form in the electronic edition of the *Astronomical Journal*.

McMath-Pierce Solar Telescope at the National Solar Observatory (NSO), which Eaton & Henry (1996) used to investigate Hα variations. Second, we have obtained 3 years' worth of red observations with the echelle spectrograph on the Tennessee State University (TSU) Automatic Spectroscopic Telescope (AST; Eaton & Williamson 2004), at Fairborn Observatory in southern Arizona. Table 1 gives measurements from the AST spectra; Table 2, from the NSO spectra. In them we list the heliocentric Julian Date of observation (HJD), the radial velocity of the G supergiant primary, and two equivalent widths of Hα. The first (EW1) is for the bulk of the profile, 6560.90–6564.75 Å in the rest frame of the star; the second (EW2) is for 6559.80–6560.90 Å. This second, blue-displaced band is designed to detect stochastic enhancements in the mass loss of the sort documented by Eaton & Henry. Figure 1 shows two representative spectra with these bands marked.

The radial velocities from the TSU AST listed in Table 1 should have random probable errors of $\sim$0.2 km s^{-1} for a broad-lined star like 22 Vul (partly intrinsic variation); they are systematically more negative than the IAU velocity system (Pearce 1957; Scarfe et al. 1990) by -0.35 km s^{-1} as measured by 2 years' observations

TABLE 2
OPTICAL SPECTRA FOR 22 VUL FROM NSO

Date (HJD−2,400,000)	RV (km s^{-1})	EW1 (Å)	EW2 (Å)	Date (HJD−2,400,000)	RV (km s^{-1})	EW1 (Å)	EW2 (Å)
48068.810	−25.1	1.716	0.187	49647.676	−39.5	1.682	0.151
48131.870	−45.3	1.887	0.204	49647.687	−39.3	1.682	0.151
48856.700	−45.5	1.803	0.103	49656.661	−35.1	1.835	0.117
49138.990	−44.3	2.083	0.158	49659.575	−34.3	1.863	0.101
49174.970	−23.7	1.678	0.118	49667.661	−26.3	1.803	0.091
49182.840	−17.7	1.679	0.109	49670.583	−26.7	1.796	0.108
49222.997	4.3	1.911	0.226	49703.570	−5.3	1.737	0.111
49281.738	−3.3	2.001	0.202	49706.610	−3.5	1.720	0.119
49302.607	−17.1	1.866	0.181	49708.547	−1.3	1.681	0.105
49326.692	−32.7	2.080	0.241	49708.561	−1.3	1.681	0.105
49340.603	−39.5	1.695	0.133	49715.564	2.5	1.638	0.094
49355.558	−44.9	1.689	0.109	49720.556	3.9	1.700	0.128
49416.031	−28.7	2.005	0.118	49768.059	−0.9	1.826	0.178
49428.011	−20.5	2.032	0.120	49769.038	−1.3	1.839	0.191
49439.999	−12.3	1.907	0.097	49769.051	−1.9	1.839	0.191
49452.002	−4.7	1.885	0.384	49776.024	−5.3	1.944	0.178
49464.962	1.5	1.827	0.255	49780.022	−10.3	1.825	0.162
49476.960	6.5	1.745	0.182	49799.964	−19.9	2.043	0.261
49487.964	8.9	1.802	0.144	49802.030	−21.5	1.946	0.221
49525.907	−5.1	1.905	0.230	49804.990	−22.3	2.016	0.206
49583.774	−37.1	1.718	0.160	49812.029	−29.7	...	...
49587.775	−42.3	1.729	0.177	49812.978	−27.1	2.004	0.147
49609.762	−48.1	1.840	0.171	49816.976	−29.7	1.961	0.120
49611.728	−48.3	1.845	0.177	49836.939	−44.3	1.870	0.247
49619.700	−47.5	1.882	0.280	49839.986	−46.5	1.873	0.208
49623.720	−49.1	1.859	0.300	49839.999	−48.5	1.873	0.208
49643.645	−40.1	1.673	0.155	49840.940	−48.7	1.874	0.211

NOTE.—Table 2 is also available in machine-readable form in the electronic edition of the *Astronomical Journal*.

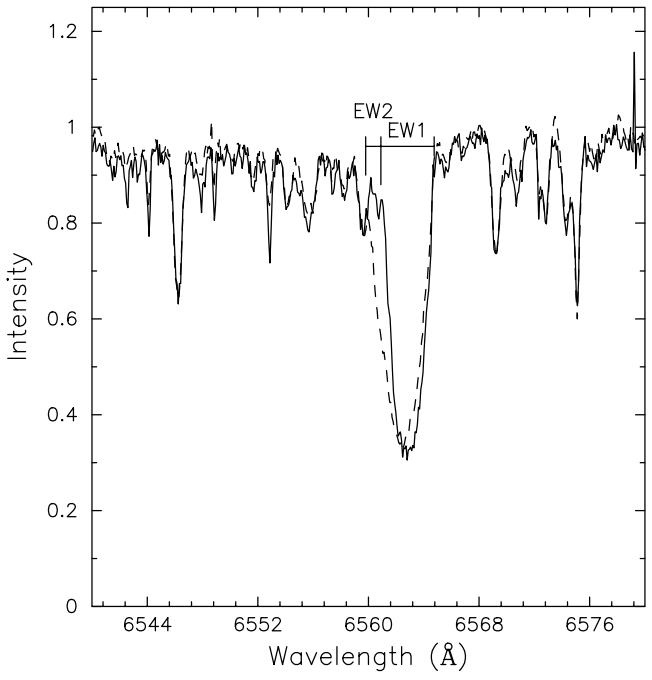

FIG. 1.—Example of the variation of the Hα profile of 22 Vul showing the two bands EW1 and EW2 we have used to quantify the strength of this line. The solid curve (JD 2,453,309) is a typical profile for such a supergiant, while the dashed curve (JD 2,452,909) shows the enhanced absorption in the blue wing that shows up episodically in cool supergiants. See Eaton & Henry (1996, Fig. 3) for this effect in ξ Cyg. The width and shape of this enhancement mean it is not caused merely by enhanced telluric lines.

of 23 standard stars (J. A. Eaton & M. H. Williamson 2007, in preparation). We have obtained a solution to our new radial velocities (Fig. 2 and Table 3). These values are, if anything, only marginally better than those of Griffin et al. (1993), but they do give a new time of conjunction, which may be used to refine the ephemeris:

$$\mathrm{HJD} = 2,453,166.98 \pm 0.05 + (249.128 \pm 0.001)\phi, \quad (1)$$

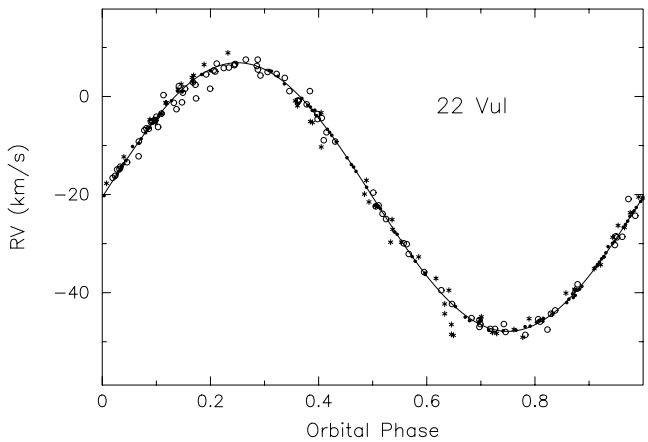

FIG. 2.—Velocity curve for 22 Vul. Dots are the new data from the TSU AST, corrected by +0.35 km s^{-1} to the IAU scale. Asterisks are observations we obtained at the NSO. Circles represent the data of Griffin et al. (1993) corrected to the IAU scale by −0.8 km s^{-1}. Only the new AST data were included in the solution represented by the solid curve; including the other data, appropriately weighted, gives the same result to within the probable errors.

TABLE 3
RESULTS OF RADIAL VELOCITY SOLUTIONS

Element	This Paper	Griffin et al.
K_{cool} (km s^{-1})	27.38 ± 0.04	27.03 ± 0.14
γ[a] (km s^{-1})	−20.50 ± 0.02	−20.60 ± 0.10
T_0[b] (HJD−2,400,000)	53229.26 ± 0.05	43014.53 ± 0.21
P[c] (days)	249.131	249.131
$a_{cool} \sin i$ ($R_\odot$)	134.2 ± 0.2	132.3 ± 0.7
σ[d] (km s^{-1})	0.27	0.66

[a] Corrected to the IAU velocity scale.
[b] At phase of maximum velocity.
[c] Assumed value from Griffin et al. (1993); see text for revision.
[d] Standard deviation of single datum from fit.

where the phase ϕ is with respect to conjunction (mid–primary eclipse). The orbit is circular to within the errors of measurement. There were no measurable lines of the B star in the red, since that component contributes only about 2% of the light there, so we can add nothing about the mass ratio. We will discuss variations of Hα in § 4.3.

3. CONSTRAINTS ON SYSTEM PROPERTIES

Because this is such a potentially interesting system, it would be nice to constrain its physical properties much better than we have in the past. The crucial element is the mass ratio, which is required to fix the geometrical elements reliably and to place the components precisely in the H-R diagram for studies of stellar evolution. Unfortunately, the only measurement of this quantity remains the necessarily crude value 1.6 ± 0.2 by Griffin et al. (1993) from measuring shifts of Balmer lines. The *IUE* spectra, in which the B star dominates, are too noisy even to detect the ∼100 km s^{-1} shift from orbital motion, much less to measure it reliably. Other constraints on the mass ratio are even more uncertain. We discuss constraints on the system parameters below.

3.1. *Spectral Type/Temperature of the B Dwarf*

This comes from ultraviolet spectra from *IUE* (Ake et al. 1985). Erhorn (1990; see Schröder 1990) compared measured ultraviolet fluxes with fluxes from Kurucz models to find an effective temperature near 10,700 K. We can compare the spectra from Ake et al. (1985, Fig. 2) with spectra of standards plotted by Wu et al. (1983) around Lyα to get a rough classification of the B star. The wings of Lyα, especially, are sensitive to temperature/spectral class. Such a comparison shows that the B star is likely B9 V; it cannot be as late as B9.5 V, although it could be B8.5 V or B8 III. The photospheric lines visible in this spectral region, although severely blended with wind features, seem consistent with that classification.

3.1.1. *Ratio of Radii from Angular Diameters*

We can get these by comparing observed flux to surface flux. Erhorn (1990) derived 0.061 mas for the B star by comparing fluxes in the ultraviolet. Griffin et al. (1993) found 1.25 mas for the G star from the Barnes-Evans relation (Barnes & Evans 1976) and optical photometry. However, they went on to correct this value for limb darkening by 3.5%–13% (to 1.29–1.37 mas). Barnes & Evans based their original relation on surface fluxes derived from occultation diameters corrected to total darkening to the limb ($x = 1.0$). This amount of darkening may actually be excessive in the deep red, where most of the diameters were measured, which would lead to surface fluxes being too low and angular diameters derived from them being too high. Therefore, any limb-darkening corrections to the measured angular diameter of 22 Vul would *lower* it ($\phi < 1.25$ mas). Naturally, we have used our own calibration of the Barnes-Evans relation (Eaton & Poe 1984), based on more data than the original, to derive an independent value for the G star, 1.37 mas [for $V = 5.21$, $(V–R)_0 = 0.76$], which gives a more realistic idea of the uncertainties involved in this sort of analysis. The ratio of radii would likely, therefore, be near the range 20.5–22.5.

3.1.2. *Fitting Eclipse Shapes*

Griffin et al. (1993) expertly pieced eclipse light curves together from various available sources and fit them with eclipses of spherical stars. They find this process is complicated by apparent atmospheric eclipses in all the optical bands and have used an attenuation model to allow for it. Given the scale of their plots showing the theoretical calculations with the data, it is hard to judge how good the fit really is. However, it seems too uncertain to restrict the mass ratio in any useful way. Also, the calculated ellipsoidal variation for their R_{cool} is too large by ∼50% with reasonable assumptions about the limb and gravity darkening.

3.1.3. *Rotational Velocity of the G Star*

If the cool star is rotating synchronously, an accurate measurement of its rotational velocity $v \sin i$ gives a meaningful constraint on the mass ratio. This is especially practical for semidetached binaries, in which the rotational velocity can be combined with the requirement that the giant component is in contact with its Roche lobe. For a *detached* system like 22 Vul, it is a much weaker constraint. Furthermore, for a component not rotating synchronously, there is no constraint at all, although, if we assume the star and chromosphere are rotating as a solid body, we can use $v \sin i$ and a measured rotational *period* to recover this constraint (see § 4.1).

3.1.4. *Ellipsoidal Light Variation*

We detected the ellipsoidal light variation of the G star (Eaton et al. 1994) and have been following it for the past 8 yr with the Vanderbilt/TSU 0.4 m automatic photometric telescope. These data are all on the same photometric system, unlike the other photometry usually analyzed, and give a very good idea of the level of ellipsoidal variation and the depth of primary eclipse at *B* and *V*. There are a few data in the partial phases of primary eclipse, which are useful for fixing the orbital inclination, but not enough to define the eclipse shape reliably.

We have fit the *B* and *V* light curves separately with the Roche model (Eaton 1975), adjusted by least squares, for assumed mass ratios in the range 1.4–2.0 with steps of 0.1. All of these solutions give roughly the same χ^2 per degree of freedom although they have a smoothly varying absolute radius for the G supergiant (Fig. 3). We have chosen to adopt a solution for $q = 1.50$ to illustrate this process and for use in the rest of this paper. Figure 4 shows how well it fits the data at *B*. The level of ellipsoidal variation detected is produced by a variation of only 1.5% in radius over the surface of the G star.

The actual computer program we used to solve the light curves is a version of the one we have used to fit light curves of a wide variety of stars over the years (e.g., Eaton & Hall 1979; Eaton 1978a, 1978b, 1978c; Eaton et al. 1993) but without any starspots. It incorporates the usual assumptions: circular orbit, synchronous rotation, rotation and revolution parallel, and that a star's photosphere coincides with an equipotential surface. (We also have a version of the program that allows for nonsynchronous rotation when appropriate.) See Eaton (1975) for definitions of the parameters of the model. We fit light curves by guessing original elements and applying a least-squares adjustment to minimize χ^2. This adjustment gives the formal errors of the fit, such as the ones

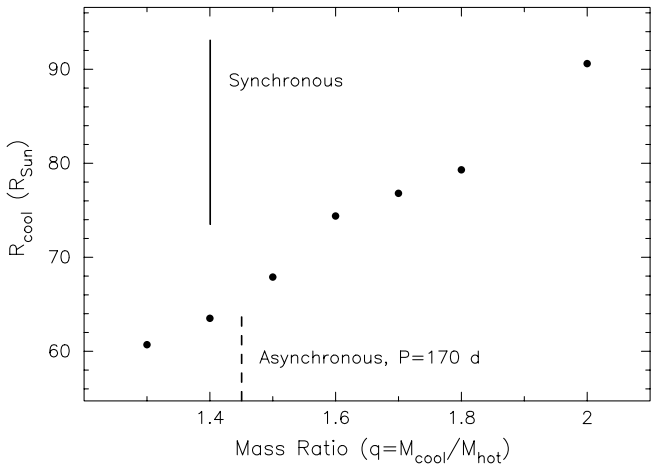

FIG. 3.—Variation of radius of the G supergiant R_{cool} with mass ratio $q = M_{cool}/M_{hot}$. The solid bar indicates the range of radius ($84.8 \pm 10\ R_\odot$) allowed by the measured rotational velocity, $v \sin i = 17 \pm 2$ km s^{-1}, for synchronous rotation. The dashed line represents the range allowed by this $v \sin i$ for *asynchronous* rotation at $P = 170$ days, $57.6 \pm 6.8\ R_\odot$.

we list in Table 4. Such formal errors almost always seem optimistic, particularly when they apply to photometrically determined mass ratios, and Popper (1984) attempted to determine just how reliable they really are by comparing formal internal errors of published solutions to externally deduced errors. His weak result suggests the formal errors are too optimistic by about a factor of 3. For this study, we have integrated the least-squares adjustment into the program that calculates light curves, although for only one wavelength at a time, instead applying it in a separate program as we have done in the past.

There is a basic logic to constraining the properties of this system. For any assumed mass ratio, the radius of the G supergiant is constrained by the ellipsoidal light variation, and the ratio of radii is constrained by an allowed range of effective temperature for each star. With these constraints applied, the inclination is determined by the duration of primary eclipse. The mass ratio itself, then, can be determined if we know $v \sin i$ and the rotational period accurately, since these two quantities give an absolute radius that maps into a mass ratio through the relation in Figure 3.

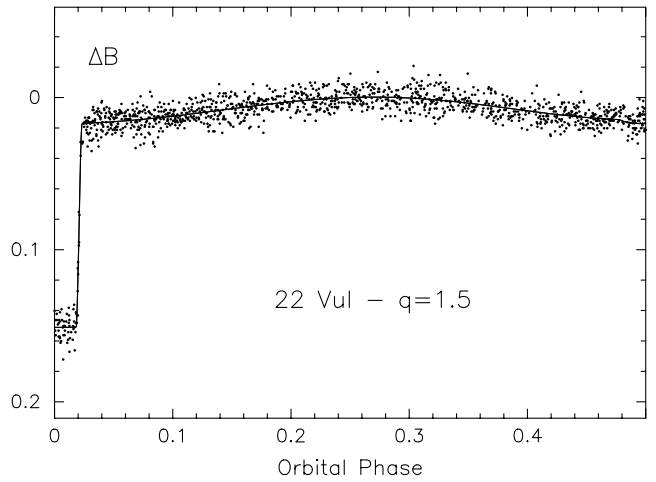

FIG. 4.—Typical fit to the blue (B) light curve from the TSU/Vanderbilt telescope. This solution is for $q = 1.50$ (Table 4). We have reflected the data about phase 0.5 and placed them on a scale with unit light at $\Delta B = -1.946$. The standard deviation for a single point in this solution is 0.0063 mag for B vs. 0.005 mag for V.

TABLE 4
RESULTS OF LIGHT-CURVE ANALYSES

Element	This Paper	Griffin et al. (1993)
$q = M_{cool}/M_{hot}$	1.50 (adopted)	1.59 (spectro)
i (deg)	81.34 ± 0.02	80.0
r_{hot}	0.0095 ± 0.0006 ($3.24\ R_\odot$)	0.0095 ($3.3\ R_\odot$)
r_{cool}	0.1990 ± 0.0014 ($67.9\ R_\odot$)	0.223 ($77\ R_\odot$)
T_{hot} (K)	10700	10900
T_{cool} (K)	4804 ± 5	4700
$\log (L/L_\odot)_{hot}$	2.09	
$\log (L/L_\odot)_{cool}$	3.34	
g_{hot}	1.00	1.00
g_{cool}	0.32	0.32
$x_{V,hot}$	0.35	0.55
$x_{V,cool}$	0.78	0.78
$x_{B,hot}$	0.43	0.55
$x_{B,cool}$	0.90	0.90
A_{hot}	1.0	1.0
A_{cool}	1.59 ± 0.14	0.5

NOTE.—The radii listed are *side* radii: 90° from the pole and line between stars, measured in units of the orbital radius.

We made the following assumptions about the binary-star model in doing these analyses: First, we used the standard convective gravity-darkening coefficient, $g = 0.32$, for the G component and linear limb-darkening coefficients, x_λ, from Al-Naimy (1978) and Claret & Gimanez (1990). Second, we treated the bolometric albedo of the G star, A_{cool}, as a wavelength-dependent fitting parameter, since the reflection effect is highly complicated and is not predictable in any simple way (n.b., Rucinski 1970). Third, we used a calibration of surface flux versus temperature from the Barnes-Evans relation (Eaton & Poe 1984) with colors for class I stars from Johnson (1966) to relate fluxes at B and V.

There are several noteworthy complications from fitting these light curves. First, we could not fit both B and V with the same temperature; the V band required a G component ~240 K hotter than B to fit the eclipse depths. We fit B and V simultaneously only by reducing the temperature to an unrealistic 4320 K, but this gave a ratio of radii (31.8) much larger than allowed by the angular diameters. This problem suggests that the Barnes-Evans relation may not hold as well for supergiants as thought. Second, the radii derived are highly dependent on assumptions about limb and gravity darkening. The limb darkening from standard model atmospheres should be reasonably good. However, the coefficients could be systematically wrong. Furthermore, Lucy's (1967) gravity darkening for convective stars ($g = 0.32$), where $T_{eff}^4 \sim (\nabla\Omega)^g$, may not be correct. This theory has never been critically tested; convective components in binaries seem to have lower gravity darkening than radiative stars, but some of them do appear to have $g > 0.32$ (e.g., Eaton 1986). This is an important complication, since x_λ, g, and r_{cool} are highly correlated. A solution with $g = 0.5$, for instance, reduced the relative radius of the cool star r_{cool} by 6%, corresponding to a change of ~0.15 in the mass ratio for a given absolute radius R_{cool}. A further complication, which we have not included in the actual fits, is the way asynchronous rotation changes the shape of the G star. Rotation more rapid than synchronous increases the tidal distortion at a given radius, but the calculated effect in this well-detached, moderately rotating system is minuscule.

3.1.5. *Masses of the Stars*

If we swallow our pride and insist that the two stars have masses appropriate for their spectral types, we get a further restriction on

TABLE 5
SOLUTIONS FOR DIFFERENT MASS RATIOS

$q = M_{cool}/M_{hot}$	M_{hot}	R_{hot}	M_{cool}	R_{cool}
2.0	5.01	4.27	10.06	90.6
1.8	4.33	3.80	7.79	79.3
1.7	4.02	3.65	6.84	76.8
1.6	3.74	3.52	5.98	74.4
1.5	3.44	3.24	5.15	67.9
1.4	3.16	3.05	4.45	63.5
1.3	2.90	2.98	3.77	60.7

the mass ratio. This comes primarily from the mass of the B9 star, which varies with mass ratio as given in Table 5. Other B8–B9.5 dwarfs have masses in the range 2.3–3.6 $M_\odot$, with an average of 2.34 $M_\odot$ for B9 V (Habets & Heintze 1981). The hot component of 22 Vul is clearly too massive for this spectral type, even for the smallest mass ratios we have considered, and its radius is larger than typical. Stellar models (e.g., Girardi et al. 2000) give luminosities like those of our hotter component [$\log (L/L_\odot) = 2.1$] for masses $\lesssim$3.5 $M_\odot$, which maps into $q \lesssim 1.5$. The luminosity of the cool star [$\log (L/L_\odot) = 3.3$] implies it is a clump giant that has already passed through the first giant branch. If this is the case, the radius ($\sim$116 $R_\odot$ at 5 $M_\odot$ per Girardi et al.) must have been rather close to the present Roche lobe radius ($\sim$140 $R_\odot$ for $q = 1.5$) in the past.

3.1.6. *Prospects for Improvement*

As we see it, the best way to improve the situation is to obtain top-quality photometry of primary eclipse, most critically in the *B* band. The existing light curve for these critical phases is poorly covered and mongrel, despite the impressive efforts of Griffin et al. (1993). Our various solutions to the light curve have shapes different enough that a well-observed eclipse ought to discriminate among them. The problem with this approach is that Griffin et al. claimed to have found atmospheric eclipse effects even at *B* and *V*, so it is not obvious that even this approach would clear up the problem of 22 Vul's mass ratio. An alternate approach would be to measure the rotational velocity much more accurately, probably by measuring violet shell lines per Griffin et al. in both ingress and egress of a single eclipse, and to determine the rotational period of the G star more precisely with better observations in the ultraviolet to chart speed with height. In the meantime, we think the best set of elements is as follows: $q = M(\text{G4 I})/M(\text{B9 V}) = 1.5$, $M(\text{G4 I}) = 5.15\ M_\odot$, $M(\text{B9 V}) = 3.44\ M_\odot$, $a = 337\ R_\odot$, $R(\text{G4 I}) = 68\ R_\odot$, $R(\text{B9 V}) = 3.24\ R_\odot$, and $i = 81.34^\circ$, which we are using in the remainder of this paper.

4. ATMOSPHERIC STRUCTURE

4.1. *Rotation of the Chromosphere*

Griffin et al. (1993) analyzed optical coudé spectra from an ingress in 1988, finding rotation of the chromosphere *faster* than synchronous. They also found a geometry roughly the same as ours, but which gives somewhat too much ellipsoidal variation. But their significant result is a $\sim$150 day rotational period for the lower chromosphere derived from shifts of chromospheric lines relative to the G star's photosphere. Since their spectra were much better exposed than the *IUE* spectra, and inasmuch as they developed meticulous procedures for manipulating them, their velocities should be more reliable. It would be surprising if the chromosphere is rotating faster than its star, yet their large radius of the G supergiant (77 $R_\odot$) is inconsistent with rotation on a 150 day period ($v \sin i = 26$ km s^{-1}). Alternatively, if 150 days is the true rotational period of the G star, the *observed* line broadening would restrict its radius to $\sim$51 $R_\odot$, a value too small to explain the observed ellipsoidal light variation or be consistent with a reasonable mass ratio (see Fig. 3).

TABLE 6
SHELL VELOCITIES FOR *IUE* SPECTRA

IUE Image	HJD	Phase	RV (Shell)
LWP 3998	45,928.16	0.9434	8.57
LWP 4007	45,929.62	0.9492	10.04
LWP 4008	45,929.81	0.9500	14.67
LWP 4016	45,930.63	0.9533	13.63
LWP 4141	45,947.84	0.0224	−6.64
LWP 4152	45,949.06	0.0273	−22.88
LWP 4186	45,952.90	0.0427	−9.02
LWP 4246	45,961.79	0.0784	−33.32
LWP 5734	46,168.93	0.9098	32.08
LWP 5774	46,173.51	0.9282	35.54
LWP 5780	46,174.92	0.9339	48.47
LWP 5812	46,180.26	0.9553	38.32
LWP 5814	46,180.32	0.9556	27.59
LWP 5820	46,181.05	0.9585	26.51
LWP 5821	46,181.12	0.9587	31.38
LWP 5844	46,184.09	0.9707	29.41
LWP 5855	46,185.07	0.9746	25.13
LWP 5867	46,185.90	0.9779	23.42
LWP 5871	46,186.15	0.9789	2.43
LWP 5958	46,197.62	0.0250	−12.86
LWP 5974	46,200.09	0.0349	−14.39
LWP 5981	46,200.63	0.0371	−18.50
LWP 5986	46,201.51	0.0406	−20.63
LWP 6011	46,205.17	0.0553	−29.54
LWP 6071	46,213.35	0.0881	−44.22
LWP15806	47,705.67	0.0783	−6.54

We have analyzed archival *IUE* spectra that track the chromosphere out much farther from the G star than optical data. These spectra also show the effects of more rapid rotation. To measure velocity shifts of wind lines, we identified 15 relatively sharp shell absorptions in the wavelength range 2450–2800 Å. These give the velocities listed in Table 6 and plotted in Figure 5. Figure 6 shows how these shifts apply to some representative spectra. These velocities clearly do not fall on the velocity curve of the B star, as they would for synchronous (solid-body) rotation without any flows projected into the line of sight. Instead, they are systematically displaced by about +20 km s^{-1} and show phase variation consistent with a rotational period of $\sim$170 days. One might expect flows in binaries to be different than in single stars because of the Coriolis effect, which actually causes mass exchange to form the disks of long-period Algol binaries. However, that deflection would make the rotation appear *slower* than synchronous. Alternatively, we might think that some peculiar radiative excitation mechanism in this wind is causing it to absorb only in certain lobes of gas with peculiarly oriented velocities, since the sharp lines we have measured are mostly from highly excited multiplets possibly subject to radiative excitation. However, a comparison of spectra from widely separated conjugate phases shows that the whole shell spectrum is shifted, not just the most highly excited multiplets (LWP 5780 and LWP 6011 are shifted by 70 $\pm$ 4 km s^{-1} in the region of Fe II UV1, versus the 78 km s^{-1} in Table 6). On the other hand, preferential radiative excitation in the gas flowing toward the B star is probably necessary to account for the systematic redshift of the shell lines we have used.

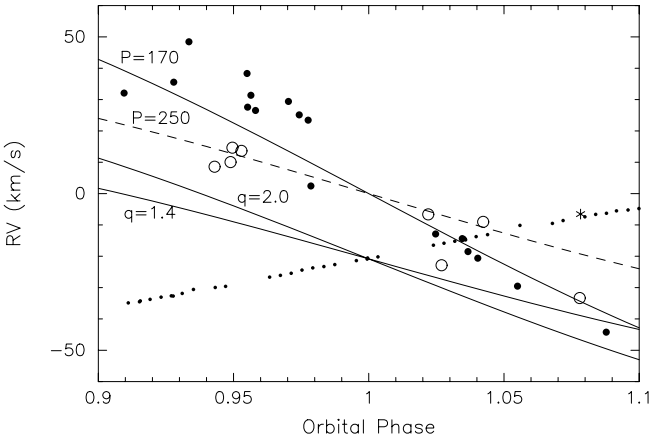

FIG. 5.—Displacements of a selected group of shell lines in archival *IUE* spectra of 22 Vul. The large symbols (*circles, large dots, and the asterisk*) represent the velocities from the ultraviolet shell lines observed during three separate atmospheric eclipses. The small dots show the optical velocity curve of the G supergiant. Two things are readily apparent: the shell lines are displaced toward positive velocity (recession) by $\sim$20 km s^{-1}, and the variation in velocity of these shell lines is much greater than expected for the B star with any reasonable mass ratio. The two lower solid curves are the expected velocity of the B star with mass ratios 1.4 and 2.0. The upper solid curve is the velocity the chromosphere would have if rotating as a solid body with a period of 170 days, displaced upward by 20 km s^{-1}; the dashed curve represents the velocity for a period of 250 days.

Since the G supergiant is almost certainly rotating faster than synchronously, what are the implications? First, this means that the system has an interesting evolutionary state, possibly having shrunk from the tip of the giant branch with approximately constant angular momentum. We shall leave it to others to speculate about what the timescale for that actually is. Second, the rotation of the chromosphere to great height implies there is momentum transport of some kind up through the outer atmosphere. This angular acceleration must add momentum to the wind in a way that more slowly rotating stars will not. The effect must be to add extra acceleration beyond the sonic point that will increase the terminal velocity of such a rapid rotator's wind. We see this in a terminal velocity ($\sim$200 km s^{-1}) that is at least as high as the surface escape velocity of the G star (170 km s^{-1}). This contrasts with other cool giants, which seem to have terminal velocities in the range 40%–60% of the surface escape velocity, even with the most generous estimates of their terminal velocities. Another rapid rotator, AL Vel (Eaton 1994), has had a wind detected at *twice* its surface escape velocity. Finally, a well-determined rotational period for the G star, combined with a more precise $v \sin i$, would give an absolute radius precise enough to restrict the mass ratio meaningfully. In Figure 3, for instance, present values, combined with a relaxation of the gravity-darkening coefficient to $g = 0.5$ to lower the plotted points $\sim 4\,R_\odot$, put the mass ratio near 1.45 ± 0.05.

4.2. *A Rediscussion of the Results from IUE*

4.2.1. *Terminal Velocity*

Zeta Aur binaries show P Cyg profiles that can give a taste of the range of velocities reached in their winds. The most useful lines tend to be Mg II *h* and *k* λ2800. These are not obviously shifted by the orbital motion and should give a reasonable lower limit to the terminal velocity.

We have made a composite of 33 archival long-wavelength *IUE* spectra and measured the edge velocities of the Mg II *h* and *k* lines in it, finding $V_{\rm edge} = -228 \pm 5$ km s^{-1}. The terminal velocity *may* be the same as the edge velocity (minus the average radial velocity of the star), provided *h* and *k* stay optically thick at the heights at which the wind quits accelerating and if there is no significant contribution to line broadening by turbulence at these levels. It is clear we may not be seeing the full velocity spread in most cool stars (e.g., Judge 1992). Furthermore, quoted terminal velocities tend to be lower than the edge velocities for these stars, often by significant amounts, because of large corrections for turbulence. However, we think this correction is wrong. First, in models for scattering in shells (e.g., Baade et al. 1996), the turbulence drops with height. Second, the logic of physics would suggest that the turbulent energy would go into accelerating the wind, or be radiated away, and be essentially damped out by the time the wind reaches its terminal velocity. Therefore, a correction for the large turbulent velocity measured in the inner wind

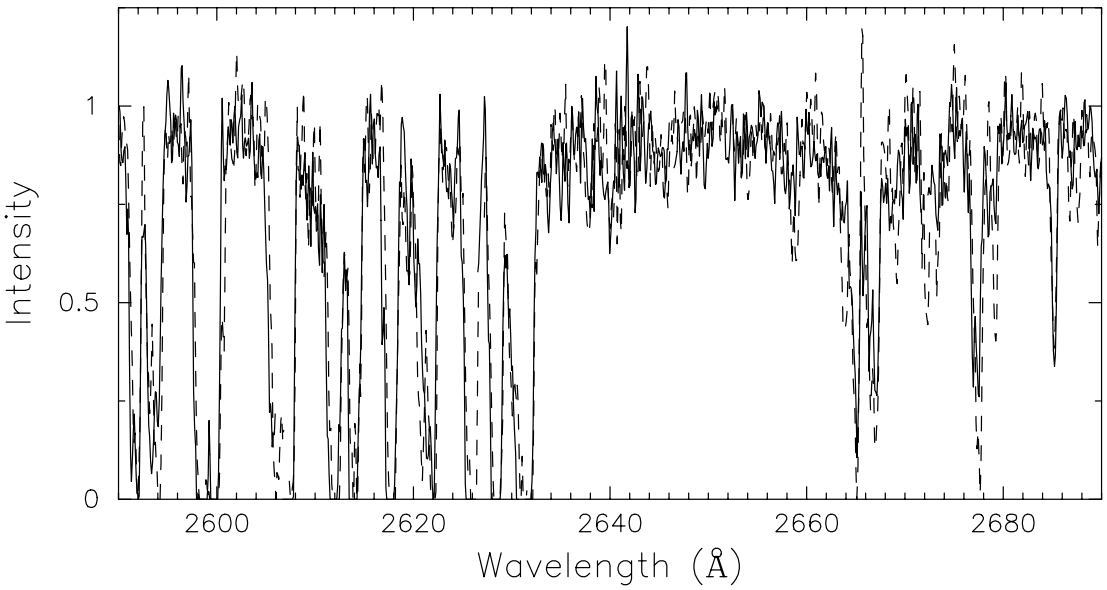

FIG. 6.—Comparison of shell spectra from opposite sides of the same primary eclipse. The solid curve represents LWP 5780, and the dashed curve represents LWP 6011 shifted 70 km s^{-1}, roughly the shift measured with the sharp shell lines. Velocities of interstellar lines in these spectra agree to 0.7 km s^{-1}. It is obvious that all of the shell spectrum participates in this apparently rotational shift of the sharp shell lines.

TABLE 7
IUE Spectra Analyzed

Epoch	Phase	Date (year day)	HJD−2,440,000	δ ($R_\odot$)	SWP Images	LWP Images	$\int \rho\, dx_{\rm H}$ (g cm^{-2})	$\int \rho\, dx_{\rm metals}$ (g cm^{-2})	$T_{\rm exc}$ (K)	$v_{\rm turb}$ (km s^{-1})
UV1	0.0212	1983 363	5698.42	67.0	21906	2527	7.3 ± 0.2	6.2 ± 1	5000	20
UV2	0.9293	1984 225	5924.66	151.2	23674	3998	0.02 ± 0.01	2.2×10^{-3}	9500	27
UV3	0.9494	1984 230	5929.67	115.3	23706	4007,4008	0.01 ± 0.003	2.1×10^{-2}	6250	27
UV4	0.9535	1984 231	5930.68	108.1	23716	4016	0.01 ± 0.002	0.075	6500	25
UV5	0.9882	1984 239	5939.32	56.2	23789	4086	...	...	...	...
UV6	0.0224	1984 248	5947.86	68.7	23869	4141	7.5 ± 2.0	2.8	4700	15
UV7	0.0264	1984 249	5948.85	74.5	23878	4152	0.22 ± 0.03	0.20	5100	22
UV8	0.0707	1984 253	5959.88	151.2	23916	4186	0.01 ± 0.005	1.5×10^{-2}	6500	25
UV9	0.0784	1984 262	5961.81	164.9	23992	4246	...	5×10^{-4}	12000	19
UV10	0.8705	1985 093	6159.13	246.3	25575	5653	0.012 ± 0.002	1.5×10^{-4}	13000	22
UV11	0.8906	1985 098	6164.13	216.5	...	5698,5699	...	2.5×10^{-4}	10000	21
UV12	0.9098	1985 103	6168.93	185.1	25678	5734	0.01 ± 0.002	5.0×10^{-4}	13000	22
UV13	0.9340	1985 109	6174.96	142.8	25736	5780	0.025 ± 0.002	1.9×10^{-3}	9000	27
UV14	0.9585	1985 115	6181.05	99.4	25775	5820,5821	0.02 ± 0.02	1.5×10^{-2}	6500	30
UV15	0.9709	1985 118	6184.14	78.7	25800	5844	0.10 ± 0.05	6.0×10^{-2}	7500	18
UV16	0.9746	1985 119	6185.07	73.0	25808,25810	5855	0.223 ± 0.04	8.3×10^{-2}	5000	11
UV17	0.9787	1985 120	6186.10	67.1	25819	5867,5871	7.2 ± 1.0	2.5	5000	20
UV18	0.0248	1985 131	6197.58	72.2	25914	5958	7.8 ± 0.2	1.0	5000	20
UV19	0.0260	1985 132	6197.87	73.9	25918	5959	...	...	...	...
UV20	0.0348	1985 134	6200.06	87.9	25934	5974	0.02 ± 0.005	2.2×10^{-2}	6200	27
UV21	0.0369	1985 135	6200.59	91.4	25941	5981	0.02 ± 0.01	2.0×10^{-2}	6500	20
UV22	0.0558	1985 139	6205.30	124.6	25979	6011	0.01 ± 0.005	9×10^{-3}	7000	22
UV23	0.0882	1985 147	6213.38	181.8	26026	6071	...	1.7×10^{-3}	10500	22
UV24	0.1274	1985 157	6223.14	243.4	26106	6155	...	2.1×10^{-3}	9500	30

would be inappropriate, and so the terminal velocity would be $v_\infty \approx v_{\rm edge} - \gamma = 208 \pm 5$ km s^{-1} for 22 Vul.

4.2.2. *Density Structure*

IUE observed 22 Vul many times, and there are a couple of good papers reporting analyses of the data record (Reimers & Che-Bohenstengel 1986; Schröder & Reimers 1989). These analyze the dominant metallic species, mostly Fe II, to determine column densities through the chromosphere/wind, fit a velocity profile, and determine a mass-loss rate. We have analyzed archival *IUE* spectra for the phases of atmospheric eclipse given in Table 7, as a student project by F. G. Shaw, with the sort of conventional one-component model used by Wilson & Abt (1954), Eaton (1993a), and Eaton & Bell (1994). In it the gas along a ray through the atmosphere of the cool supergiant is characterized by (1) a mass column density, (2) a single excitation temperature, and (3) a single turbulent velocity beyond the turbulence of thermal motions at the excitation temperature. This characterization is clearly too simple for actual stars, as we have argued in Eaton & Bell, but it gives us a way to draw at least some meaningful inferences from atmospheric eclipses. In particular, we can use the damping wings of Lyα to deduce a column density of atomic hydrogen in the wind that should be more meaningful in some parts of the atmosphere than the column densities derived from singly ionized metals.

Table 7 also gives results from measurements of these spectra. Listed there are measurements of RHOX $= \int \rho\, dx$ along a ray through the chromosphere a distance δ from the center of the G supergiant. Figure 7 shows the variation of this column density with distance from the center of the G star. The Lyα column densities seem to become immeasurable at $\lesssim$0.01 g cm^{-2}. The whole density profile seems consistent with a $\beta = 2.5$–3.5 velocity profile, where

$$v(r) = v_\infty (1 - R_*/r)^\beta \qquad (2)$$

and the density ρ is as usual given by the equation of continuity, $\dot{M} = 4\pi r^2 \rho v(r)$. The three density profiles represent very different rates of acceleration, with $\beta = 1$ reaching one-half terminal velocity at twice the stellar radius. These profiles require rather different mass-loss rates to match the data at RHOX = 0.01, as we have here, ranging over an order of magnitude. For $\beta = 2.5$, $\dot{M} \sim 1.6 \times 10^{-8}\ M_\odot$ yr^{-1}, about the same as found by Schröder & Reimers. It represents a surface mass flux only 4 times as great as Eaton & Bell found for 31 Cyg.

The excitation temperatures derived for the wind are similar to those in other ζ Aur binaries. Figure 8 shows the variation with

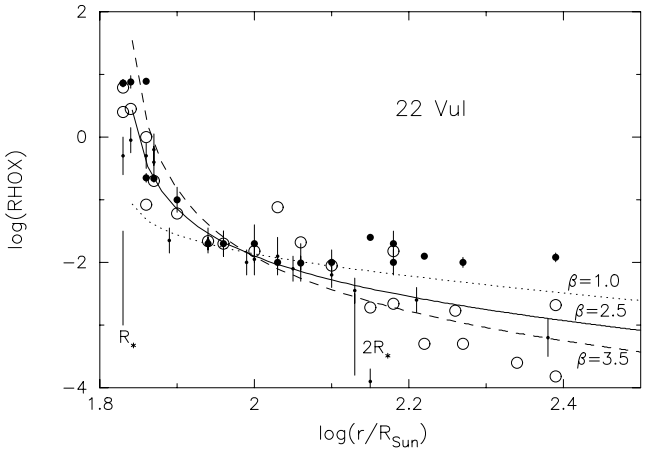

Fig. 7.—Mass column density of the wind with distance from the center of the G star measured in *IUE* spectra. Large dots represent values from the wings of Lyα, which seem to saturate above 90 $R_\odot$. Circles represent the values we deduced from metallic lines, and small dots represent measures from Schröder & Reimers (1989). The solid line represents a model with $\beta = 2.5$, a terminal velocity of 200 km s^{-1}, and a mass-loss rate of $1.6 \times 10^{-8}\ M_\odot$ yr^{-1}; the dashed line represents a model with $\beta = 3.5$ and $\dot{M} = 6.1 \times 10^{-9}\ M_\odot$ yr^{-1}; and the dotted line represents a model with $\beta = 1.0$ and $\dot{M} = 6 \times 10^{-8}\ M_\odot$ yr^{-1}.

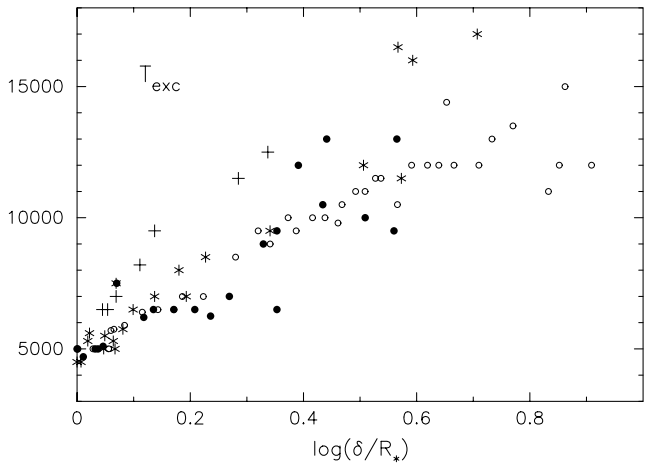

FIG. 8.—Excitation temperature vs. radius in four ζ Aur binaries. Data are represented by dots for 22 Vul, circles for 31 Cyg (Eaton & Bell 1994), asterisks for 32 Cyg (Eaton 1993b), and plus signs for ζ Aur (Eaton 1993a). These temperatures apply to gas somewhat above the radius corresponding to δ, the radius projected onto the sky.

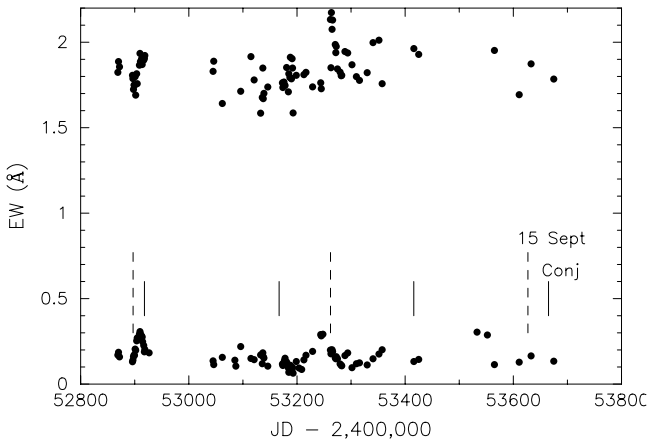

FIG. 9.—Variation of the blue wing of Hα in 22 Vul. At the top is the full profile, EW1 in Table 1, and at the bottom, the blueshifted band, EW2, designed to detect profile variations. Data from the AST and NSO (not plotted) give the same average values for these two bands, 1.84 and 0.17 Å, respectively. The vertical lines represent times of conjunction with the G star in front and 15 September in each year, roughly the date when the humidity drops and the weather improves enough for the photometric telescopes at Fairborn Observatory to start observing after a summer shutdown.

height in four of these systems. Turbulence, which is derived from fitting line strengths as in a traditional curve-of-growth analysis, seems to be similar to that in other systems, as well.

4.3. Hα *Variations as a Measure of Wind Variation*

The large strength of hydrogen lines seen in cool giants and supergiants is a direct indication that these stars have chromospheres, and the column densities of these chromospheres are so great in the supergiants that the core of Hα seems to be formed in the wind (Mallik 1993). In 31 Cyg, for instance, we have detected Hε absorption out to $1.4R_*$ beyond the limb, and observations of M supergiants also find Hα emission coming from an area approximately twice the diameter of the stellar disk (e.g., White et al. 1982; Hebden et al. 1987). Figure 9 shows the variation of our blueward-displaced band, EW2, over the last 2 years. See Eaton & Henry (1996, Fig. 4) for the earlier data. Data from both the NSO and the AST show apparently episodic profile variations. There were several in the earlier NSO data in which EW2 increased by 0.1–0.2 Å, and we see a couple more in the denser AST data. These are not obviously correlated with the orbital phase. Nor do they appear only at certain seasons of the year, as they would if caused by telluric lines. The two episodes in the AST data are at HJD 2,452,910 and HJD 2,453,250. They have durations of 20–70 days, enough time for gas $1R_*$ above the surface to move 50–150 $R_\odot$. Inspection of plots of the lines shows that there are enhancements of the blue wing of Hα at these times, that is, the lines actually look broader (see, e.g., Fig. 1). Telluric lines are probably not causing the first of them, as judged by relative strengths of such lines in the Sun (Moore et al. 1966), but that they *could* be a contributor to the second.

Such episodic Hα variations are a *global* phenomenon, as Mallik's calculations presuppose. The gas producing the extra absorption cannot be covering only a small fraction of the surface of the G star; it must cover the entire face and emerge globally within ∼10 days to maintain the coherence of the phenomenon. Thus, it is unlikely that it is associated with supergranulation, unless a supergranule can cover most of a given face of the star.

5. CONCLUSIONS

We have reanalyzed the existing body of spectroscopy and photometry for 22 Vul to try to constrain the physical properties of its components better. We find that the ratio of masses of the components is likely in the low end of the range determined spectroscopically by Griffin et al. (1993), being near 1.5. If we make some further assumptions about gravity darkening and require the rotation of the chromosphere to agree with the measured rotational velocity of the star, the mass ratio is likely in the range 1.45 ± 0.05, but this value seems overly speculative at this time. We have analyzed archival *IUE* spectra to determine properties of the G star's wind, most notably by using the wings of Lyα to measure column densities in the inner chromosphere and Fe II excitation to derive the excitation temperature throughout the chromosphere/wind. The measured values are similar to those in the outer atmospheres of other ζ Aur binary components. This star is potentially interesting in that it is a very rapid rotator for its spectral type, seems to be on a loop from the giant branch, and is probably rotating more rapidly than synchronously.

We thank Greg Henry for collecting the photometry with the Vanderbilt/TSU automatic photometric telescope. This research has been supported by grants NASA NCC5-511 and NSF HRD-9706268.

REFERENCES

Abt, H. A. 2006, ApJ, 651, 1151
Ake, T. B., Parsons, S. B., & Kondo, Y. 1985, ApJ, 298, 772
Al-Naimiy, H. M. 1978, Ap&SS, 53, 181
Baade, R., Kirsch, T., Reimers, D., Toussaint, F., Bennett, P. D., Brown, A., & Harper, G. M. 1996, ApJ, 466, 979
Barnes, T. G., & Evans, D. S. 1976, MNRAS, 174, 489
Claret, A., & Gimanez, A. 1990, A&A, 230, 412
Eaton, J. A. 1975, ApJ, 197, 379
Eaton, J. A. 1978a, Acta Astron., 28, 63
———. 1978b, Acta Astron., 28, 195
———. 1978c, Acta Astron., 28, 601
———. 1986, Acta Astron., 36, 79
———. 1990, Inf. Bull. Variable Stars 3460
———. 1993a, ApJ, 404, 305
———. 1993b, AJ, 105, 1525
———. 1994, AJ, 107, 729

Eaton, J. A., & Bell, C. 1994, AJ, 108, 2276
Eaton, J. A., & Hall, D. S. 1979, ApJ, 227, 907
Eaton, J. A., & Henry, G. W. 1996, in IAU Symp. 176, Stellar Surface Structure, ed. K. G. Strassmeier & J. L. Linsky (Dordrecht; Reidel), 415
Eaton, J. A., Henry, G. W., Bell, C., & Okorogu, A. 1993, AJ, 106, 1181
Eaton, J. A., Henry, G. W., & Seeds, M. A. 1994, in ASP Conf. Ser. 64, Eighth Cambridge Workshop on Cool Stars, Stellar Systems, and the Sun, ed. J.-P. Caillault (San Francisco: ASP), 696
Eaton, J. A., & Poe, C. H. 1984, Acta Astron., 34, 97
Eaton, J. A., & Williamson, M. H. 2004, Proc. SPIE, 5496, 710
Erhorn, G. 1990, Ph.D. thesis, Univ. Hamburg
Girardi, L., Bressan, A., Bertelli, G., & Chiosi, C. 2000, A&AS, 141, 371
Griffin, R. E. M., Hünsch, M., Marshall, K. P., Griffin, R. F., & Schröder, K.-P. 1993, A&A, 274, 225
Habets, G. M. H. J., & Heintze, J. R. W. 1981, A&AS, 46, 193
Hebden, J. C., Eckart, A., & Hege, E. K. 1987, ApJ, 314, 690
Johnson, H. L. 1966, ARA&A, 4, 193
Judge, P. G. 1992, in ASP Conf. Ser. 26, Seventh Cambridge Workshop on Cool Stars, Stellar Systems, and the Sun, ed. M. S. Giampapa & J. A. Bookbinder (San Francisco: ASP), 403
Lucy, L. B. 1967, Z. Astrophys., 65, 89
Mallik, S. V. 1993, ApJ, 402, 303
Moore, C. E., Minnaert, M. G. J., & Houtgast, J. 1966, The Solar Spectrum 2935 to 8770 Å (Washington: USGPO)
Parsons, S. B., Ake, T. B., & Hopkins, J. L. 1985, PASP, 97, 725
Pearce, J. A. 1957, Trans. IAU, 9, 441
Popper, D. M. 1984, AJ, 89, 132
Reimers, D., & Che-Bohenstengel, A. 1986, A&A, 166, 252
Rucinski, S. M. 1970, Acta Astron., 20, 327
Scarfe, C. D., Batten, A. H., & Fletcher, J. M. 1990, Publ. Dominion Obs. Ottawa, 18, 21
Schröder, K.-P. 1990, A&A, 236, 165
Schröder, K.-P., & Reimers, D. 1989, A&A, 208, 223
White, N. M., Kreidel, T. J., & Goldberg, L. 1982, ApJ, 254, 670
Wilson, O. C., & Abt, H. A. 1954, ApJS, 1, 1
Wright, K. O. 1970, Vistas Astron., 12, 147
Wu, C.-C., et al. 1983, *IUE* NASA Newsl. 22